Influence of nozzle geometry and injection conditions on the cavitation flow inside a diesel injector

A. Zandi[1], S.Sohrabi[2] , M. Shams[3]

1,2-MSc Graduated 3Associated Professor, Faculty of Mechanical Engineering, K.N. Toosi University of Technology, Tehran, Iran

Abstract

Cavitation and turbulence in a diesel injector nozzle has a great effect on the development and primary breakup of spray. However, the mechanism of the cavitation flow inside the nozzle and its influence on spray characteristics have not been clearly known yet because of the internal nozzle flow complexities. In this paper, a comprehensive numerical simulation is carried out to study the internal flow of nozzle and the cavitation phenomenon. The internal cavitation flow of the nozzle is simulated using the Eulerian-Eulerian two-fluid model. In this approach, the diesel liquid and the diesel vapor are considered as two continuous phases, and the governing equations of each phase are solved separately. Simulation method is validated by comparing the numerical results with experimental data and good correspondence is achieved. The effective parameters on the nozzle flow are investigated, including injection pressure, back pressure, inlet curvature radius of orifice, orifice iconicity and its length. Results clearly show the importance of nozzle geometrical characteristics and dynamic parameters on the internal nozzle flow. Discharge coefficient of nozzle and cavitation distribution in the nozzle are extremely dependent on these parameters, so the effect of cavitation on the primary breakup is not negligible.

***Keywords**: Diesel injector, cavitation, turbulence, multi-fluid model, nozzle geometry.*

1. Introduction

Formation and activity of bubbles in a liquid is called cavitation. This phenomenon starts from voids or tiny bubbles containing gas or vapor. If these bubbles are exposed to a pressure less than the vapor pressure, they rapidly grow. As the surrounding pressure increases to values higher than the vapor pressure, these bubbles become unstable and collapse [1]. Increasing the injection pressure in modern diesel engines produces higher pressure gradients and shear stresses in the injector nozzle [2]. With a sudden decrease in the cross section of the nozzle orifice inlet, a low-pressure region in the inlet is created, and as the flow accelerates, the local pressure drops to values lower than the vapor pressure, so bubbles appear. Cavitation is undesirable in industrial devices such as valves, pumps, etc.; because it decreases the efficiency and causes surface damages in these systems. In diesel injector nozzles, cavitation can be useful because it can improve the fuel spray atomization. The purpose of fuel spray is to enhance the surface area of the liquid, and consequently, to increase heat and mass transfer rate, since it causes the air and fuel to mix better [3]. Experimental and numerical studies have shown that spray atomization is divided into two steps, primary and secondary breakup [4-7]. The primary breakup which takes place in near-the-nozzle field is not only influenced by the interaction between the liquid jet and the surrounding gas; it is also affected by some other phenomena such as turbulence and cavitation inside the injector nozzle too [8, 9]. If the bubbles inside the nozzle are able to reach the exit and collapse, the breakup of the jet will increase [10, 11]. In addition, cavitation increases the nozzle flow velocity for two reasons. First, because of the presence of vapor alongside the nozzle wall, the liquid will not have a no-slip condition boundary, second, because there are vapor in the nozzle, its effective area decreases [12]. So, cavitation is expected to improve the spray development and lead to complete combustion of the fuel, reduction in fuel consumption, and reduction in pollutants and particulate matters.

Although cavitation results in a better spray atomization, it has some disadvantages too. More cavitation reduces the efficiency (discharge coefficient) of the nozzle. On the other hand, imploding of bubbles in the nozzle causes the erosion of its internal surface and decreases its lifetime [13]. Because of the mentioned reasons, complete

understanding of the nozzle flow physics is extremely necessary for predicting characteristics of the spray and behavior of the breakup which have crucial roles in design of efficient nozzles, engine performance, and production of pollutants. Important factors in cavitation are divided into two categories, geometrical and dynamic. Type of the nozzle (Minisac or Valve covered orifice), inlet curvature radius of the orifice, length of the orifice, and orifice conicity are important geometrical parameters, and injection pressure, back pressure, and needle eccentricity are important dynamic parameters.

Unfortunately, because of some inherent complexities like occurrence of cavitation and turbulence of the flow, it is hard to understand the physics of the flow inside the nozzle. High injection pressure together with small dimensions of the nozzle (with a diameter btween 100-200 μ m, and approximate length of 1 mm) and the injection time of 1-2 ms produce a flow with a velocity of several hundred meters per second, which is extremely transient and completely turbulent. These conditions make the experimental observation of cavitation in a real size nozzle very hard and expensive. However, considerable efforts have been made to understand the cavitation phenomenon in the nozzle and its effect on the spray atomization. In the following,

a review over the experimental studies in the field of cavitation in injector nozzles is presented.

The relation between cavitation and diesel injection was investigated first by Bergwerk in his excellent paper [14]. Bergwerk studied the flow through small transparent nozzles and pointed out the presence of cavitation and hydraulic flip in them. The Effect of cavitation on the discharge coefficient was investigated by Nurick [15]. He established a relationship between the discharge coefficient, injection pressure and back pressure. He explained the behavior of the experimental data using a one-dimensional analytical model extracted from Bernoulli ' s equation. Later studies showed that cavitation is a transient, multi-dimensional phenomenon. Chaves et al. found out that supercavitation results in a sudden increase in the spray angle [4].

Soteriou et al. by conducting experiments on large scale nozzles showed that cavitation behavior is different from that of real scale nozzles. Nevertheless, they showed that discharge coefficient is independent of the nozzle scale. They, also, observed that the flow behavior in the orifice depends on upstream features, such as the flow around the needle and sac [16]. The effect of cavitation on turbulence in high-pressure nozzles was studied by He and Ruiz [17]. Badock et al. experimentally showed that increasing the conicity and inlet curvature of the orifice decrease cavitation [18]. Arcoumanis et al., by doing experiments on scaled-up nozzles, showed that cavitation does not scale up [19]; as a result, real scale nozzles are needed to investigate the characteristics of a cavitational flow, so in the later studies, real size nozzles have been used. Comprehensive researches on the cavitational flow inside simple geometry nozzles have been done by Winklhofer et al. [20]. They experimentally measured some flow parameters like volume fraction, mass flow rate and the velocity field by investigating cavitation in different back pressures. Benajes et al. showed that the discharge coefficient in convergent orifices is higher than that of cylindrical orifices [21]. Also, Payri et al. discovered in their studies that increasing conicity of the orifice results in increasing tip penetration of the spray [22]. Roth et al. did some numerical and experimental studies to investigate the effect of using multiple injection methods on the cavitation and observed that cavitation patterns in major and pilot injections are similar [23]. Powell et al. [24] used phase-enhanced imaging to ascertain the real geometry of a single-hole nozzle and the detailed motion of the needle. They used the resulting geometry to make a computational grid of the nozzle. The internal flow of the nozzle was then simulated at different stages of the injection process.

Results showed that radial displacement of the needle can affect the flow pattern in the nozzle sac. Payri et al. [25] performed a combined experimental and numerical study to investigate the ability of a computational model in predicting the experimental behavior of the nozzle. They proved that the model is capable of reproducing the experimental data such as mass flow rate and spray momentum flux. Influence of different diesel fuels on the cavitation volume inside the nozzle was studied by Lockett et al. [26] using fast video photography of elastic light scattering.

In addition to the mentioned experimental studies, nowadays, using numerical simulations have become popular for studying the flow inside the nozzle. There are different approaches for simulating cavitation. A complete review over all of these approaches has been done by Giannadakis [27]. Among all these approaches, there are two major methods for simulating cavitational flow inside the nozzle as follow:

1. The homogeneous equilibrium models (HEMs) in which the fluid flow is assumed to be a homogeneous mixture of two phases. In HEMs, the amount of cavitation is expressed by the vapor mass fraction which has a value between zero and one. In

these models, cavitation growth is calculated using an equation of state which relates mixture pressure and density. HEMs depending on the formulation of state equation and pressure equation have different types [12].

2. The two-fluid models in which the vapor and liquid phases are treated separately, and the governing equations are solved for each phase, and the interaction between the phases are modeled using additional terms. Two-fluid models can be divided into two groups, Eulerian−Eulerian and Eulerian−Lagrangian. The Eulerian−Eulerian models are the most common methods in simulating multiphase flows. In principle, any multiphase flows can be simulated in this way. The Eulerian − Lagrangian models are alternatives for Eulerian−Eulerian models and are often used for simulating highly dispersed flows in which the volume fraction of the dispersed phase is small [12].

In this study, the cavitational flow inside an injector nozzle is simulated using Eulerian−Eulerian two-fluid model. The commercial CFD software, AVL-Fire was used to perform the numerical simulation [28]. In the present work, the effect of dynamic and geometrical parameters such as injection pressure, back pressure, inlet curvature radius of the orifice, the orifice conicity, and its length on the cavitation phenomenon is investigated. The calculated data at the outlet of the nozzle can be used as boundary conditions for simulating the spray primary breakup, combustion and pollutant production in a diesel engine. Using these data, a quasi dynamic coupling can be created between the inside flow of nozzle and the spray atomization. So, the effects of the inner nozzle flow on the spray atomization could be investigated which is our next research subject.

This study is organized in seven parts. In the second part, computational model and governing equations are presented. The third section is devoted to introducing some non-dimensional numbers important for describing the internal nozzle flow. In the fourth part, the computational model is validated by using experimental data. In the fifth section, computational domain and the operating conditions are presented. Simulation results are presented and discussed in the sixth section. Finally, conclusions are provided in the seventh section.

2. Computational model

The cavitational flow inside the nozzle is simulated by using Eulerian multi-fluid method, which can be applied to n-phase flows. In this paper, a two-phase flow is considered, which comprises diesel liquid and diesel vapor. The flow is assumed isothermal. According to Eulerian−Eulerian approach each phase is considered as a continuous medium. In this approach, the interfacial exchanges establish the coupling between phases. The interfacial interaction models are achieved through applying an ensemble averaging procedure on the governing equations [28].

2.1. Conservation equations

In the present work, the transport equations consist of conservation equations of mass and momentum.

Because of the isothermal condition the energy equation is omitted. For each phase a set of conservation equations is solved. These equations for phase are described as follows [29]:

Mass conservation equation:

$$\frac{\partial \alpha_k \rho_k}{\partial t} + \nabla . \alpha_k \rho_k \vec{v}_k = \sum_{l=1, l\neq k}^{2} \Gamma_{kl} \quad (1)$$

Where, α is volume fraction, ρ is density, $\vec{v}$ is velocity, and Γ is the interfacial mass transfer. The compatibility condition must be observed:

$$\sum_{k=1}^{2} \alpha_k = 1$$

Momentum conservation equation:

$$\frac{\partial \alpha_k \rho_k \vec{v}_k}{\partial t} + \nabla . \alpha_k \rho_k \vec{v}_k \vec{v}_k = -\alpha_k \nabla p + \nabla . \alpha_k \left(\vec{\tau}_k + \vec{T}_k^t\right) + \alpha_k \rho_k \vec{f}_k + \sum_{l=1, l\neq k}^{2} \vec{M}_{kl} + \vec{v}_k \sum_{l=1, l\neq k}^{2} \Gamma_{kl} \quad (2)$$

Where, p is pressure, $\vec{\tau}$ is viscous shear stress, $\vec{T}^t$ is Reynolds stress, $\vec{f}$ is body force, and $\vec{M}$ is the interfacial momentum transfer. Pressure is assumed identical for two phases.

2.2 Turbulence model

According to the high injection pressure, the flow Reynolds number inside the nozzle is above 20,000, hence the flow is fully turbulent. In this paper, $k-\varepsilon$ turbulence model is used for modeling Reynolds stresses appeared in the averaged Navier Stokes equations. Turbulence kinetic energy equation and

turbulence dissipation equation for phase k are as follows [30]:

Turbulence kinetic energy equation:

$$\frac{\partial \alpha_k \rho_k k_k}{\partial t} + \nabla . \alpha_k \rho_k \vec{v}_k k_k = \nabla . \alpha_k \left(\mu_k + \frac{\mu_k^t}{\sigma_k}\right) \nabla k_k + \alpha_k P_k - \alpha_k \rho_k \varepsilon_k + k_k \sum_{l=1, l\neq k}^{2} \Gamma_{kl} \quad (3)$$

Turbulence dissipation equation:

$$\frac{\partial \alpha_k \rho_k \varepsilon_k}{\partial t} + \nabla . \alpha_k \rho_k \vec{v}_k \varepsilon_k = \nabla . \alpha_k \left(\mu_k + \frac{\mu_k^t}{\sigma_\varepsilon}\right) \nabla \varepsilon_k + \alpha_k C_1 P_k \frac{\varepsilon_k}{k_k} - \alpha_k C_2 \rho_k \frac{\varepsilon_k^2}{k_k} - \alpha_k C_3 \rho_k \varepsilon_k \nabla . \vec{v}_k + \varepsilon_k \sum_{l=1, l\neq k}^{2} \Gamma_{kl} \quad (4)$$

Where, k is turbulence kinetic energy, μ is dynamic viscosity, μ^t is turbulent viscosity, and ε is turbulence dissipation. P is the production term of the viscous forces:

$$P_k = \vec{T}_k^t : \nabla \vec{v}_k \ , \ k = 1,2 \quad (5)$$

In equations (3) and (4), σ_k, σ_ε, C_1, C_2 and C_3 are closure coefficients [30]. Turbulence viscosity of continuous phase is calculated by adding bubble induced viscosity $\nu_c^{t,BI}$ to the shear induced turbulent viscosity $\nu_c^{t,SI}$ [31].

1.3 Cavitation model

With applying the two-fluid model, the cavitation inside the nozzle is simulated. Relevant interfacial exchange terms are the interfacial mass exchange and the interfacial momentum exchange.

Interfacial mass exchange:

The rate of mass exchange between phases is calculated by using bubble dynamics. This rate describes the isothermal evaporation or condensation between two phases and can be modeled with the following equation [28]:

$$\Gamma_c = \rho_d N''' 4\pi R^2 \dot{R} = -\Gamma_d \quad (6)$$

In which, N''' is bubble number density, and R is bubble radius. Subscripts c and d denote the continuous (liquid) and dispersed (vapor) phases, respectively. The rate of bubble deformation is estimated from the Rayleigh-Plasset equation [32]. Bubble number density is calculated according to an empirical formula [33].

Interfacial momentum exchange:

The effects of drag and turbulent dispersion forces are considered to determine the momentum exchange between liquid and vapor phases. Equation (7) is applied to determine the interfacial momentum exchange [28]:

$$\vec{M}_c = C_D \frac{1}{8} \rho_c A''' |\vec{v}_r| \vec{v}_r + C_{TD} \rho_c k_c \nabla \alpha_d = -\vec{M}_d \quad (7)$$

Where, C_D is drag coefficient, C_{TD} is the turbulent dispersion coefficient, A''' is the interfacial area density, and $\vec{v}_r$ is the relative velocity between phases. Drag coefficient is calculated by using a correlation, suggested by Ishii [34]. The interfacial area density for bubbly flow equals:

$$A''' = \pi D_b^2 N''' = (36\pi)^{\frac{1}{3}} N'''^{\frac{1}{3}} \alpha_d^{\frac{2}{3}} \quad (8)$$

Where, D_b is bubble diameter and it is uniquely defined by using the bubble number density and volume fraction of the dispersed phase:

$$D_b = \left(\frac{6\alpha_d}{\pi N'''}\right)^{\frac{1}{3}} \quad (9)$$

As overview the first and second terms in equation (7) represent the momentum exchange between two phases due to drag force and turbulent dispersion force, respectively. Turbulent dispersion force takes into account the effect of vapor diffusion due to turbulent mixing processes. In this paper, C_{TD} is set to 0.1.

3.Nozzle flow coefficients

The flow inside the nozzle is characterized by the discharge coefficient. The discharge coefficient is defined as the ratio of the real mass flow rate to the theoretical mass flow rate:

$$C_d = \frac{\dot{m}}{\dot{m}_{th}} = \frac{\dot{m}}{A_{th}\sqrt{2\rho_f (p_{inj} - p_{back})}} \quad (10)$$

Where, $\dot{m}$ is the real mass flow rate which can be calculated from the nozzle flow simulation. A_{th} is the

nozzle outlet area, ρ_f is the density of the liquid phase, p_{inj} is the injection pressure (upstream pressure), and p_{back} is the back pressure (downstream pressure). In this study, cavitation is characterized by cavitation number$K$:

$$K = \frac{p_{inj} - p_{vapor}}{p_{inj} - p_{back}} \quad (11)$$

In which, p_{vapor} is the vapor pressure of liquid phase. This non dimensional parameter increases by decreasing the injection pressure or increasing the back pressure.

4. Validation of computational model

The computational model is validated by comparing the numerical results with experimental data from Ref. [16]. These experiments were carried out on a simple geometry nozzle. Figure 1 shows the geometry of the cylindrical nozzle with its inlet and outlet chambers. The length of the outlet chamber is assumed to be seven times longer than that of the nozzle to reduce the effects of the external flow on the internal nozzle flow. The geometry and the computational grid were made by using GAMBIT 2.4.6 software. Pressure boundary conditions are applied at both inlet and outlet. The internal flow of the nozzle is simulated at different injection pressures. In all cases, the back pressure is fixed to 3 MPa, and the injection pressure is varied from 6 MPa to 60 MPa. A wide range of cavitation numbers between 1.05 and 2.50 is investigated using aforementioned inlet and outlet pressures. Fuel properties are presented in Table 1. Simulation results and experimental data are presented in Figure 2. The vertical axis represents the discharge coefficient, and the horizontal axis represents the cavitation number (K). Numerical results closely follow the variation path of the experimental data. At higher values of K, because there is no cavitation or it does not develop to the nozzle outlet, the discharge coefficient remains constant. As the K decreases and reaches to the approximate number of 1.4, the discharge coefficient starts to decrease. The reason is that the cavitation develops to the outlet of the nozzle which decreases the outlet area. The cavitation number related to this point is called critical cavitation number.

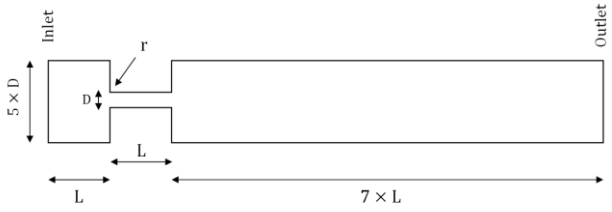

D (μm)	L (μm)	r (μm)
275	1000	0

Fig1. Schematic of the cylindrical nozzle and its dimensions.

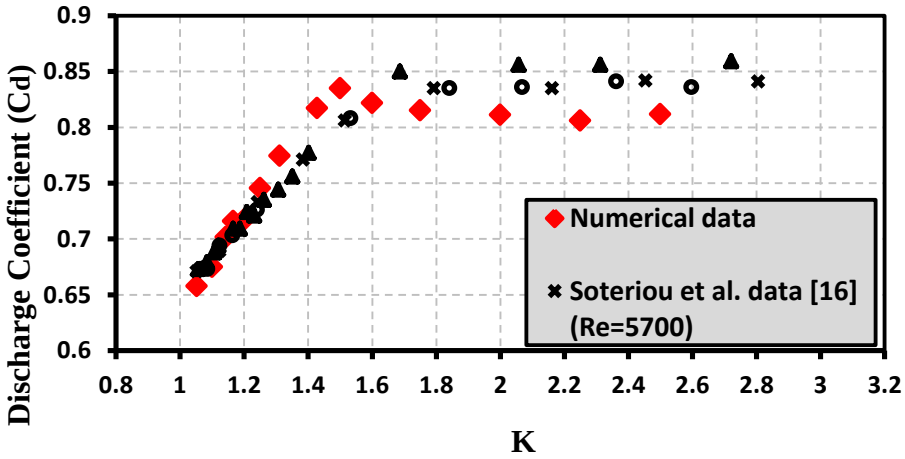

Fig2. Diagram of the discharge coefficient of simple geometry nozzle with respect to the cavitation number.

Table 1. Fuel properties (at 40℃) [36, 37].

Fuel	Liquid Density (kg/m^3)	Liquid Viscosity (Pa s)	Vapor Density (kg/m^3)	Vapor Viscosity (Pa s)	Saturation Pressure (Pa)
EU Diesel	825	0.0021	0.05	1e-5	1000

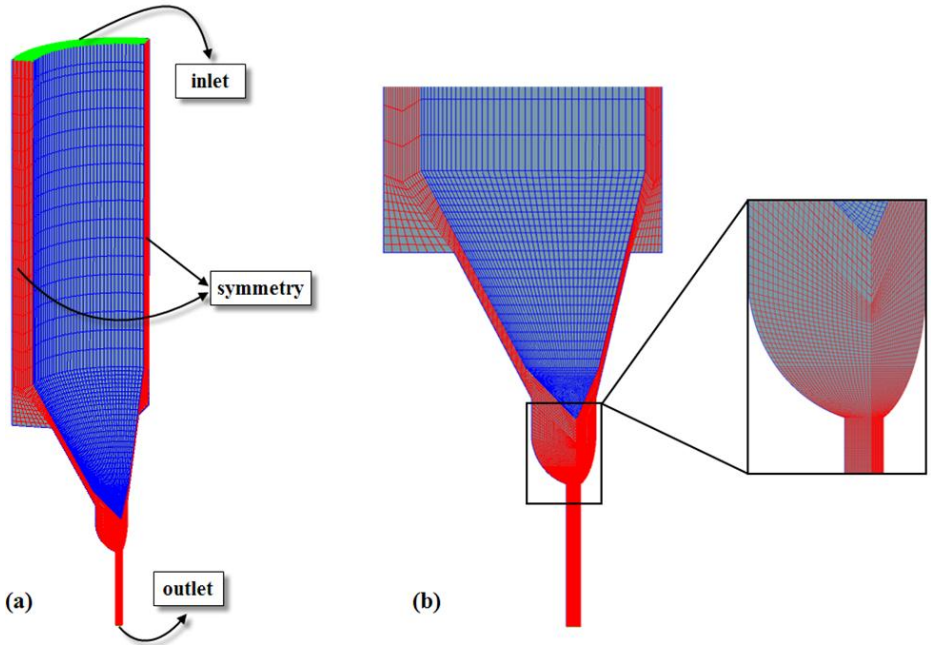

Fig3. Generated mesh for numerical solution. (a), General view (b), Grid at the inlet of the orifice.

5. Grid description and operating conditions

In this paper, a single-hole minisac nozzle is investigated. Figure 3 shows the geometry and computational domain of the base nozzle which is created in GAMBIT 2.4.6 software. Because of the geometrical symmetry of the nozzle, only a 90° sector is modeled. Pressure boundary conditions are applied at the inlet and outlet of the nozzle and symmetry boundary conditions are applied to both sides of the model (see Figure 3(a)). As shown in Figure 3(b), because of high gradient flow at the inlet of the orifice, a very fine mesh is used in this area. The geometrical parameters of the nozzle orifice are presented in Figure 4. In which, D_{in} and D_{out} are the inlet and outlet diameters, r is the inlet curvature radius, and L is length. The inlet and outlet diameters and length of the base nozzle orifice are 150 μm and 1 mm, respectively, and its inlet edge is considered to be sharp (r = 0). Grid independency of the base nozzle is investigated by studying the effect of the grid size on the outlet mass flow rate. In order to study the grid independency, five different grids are used. Variations of the mass flow rate of the liquid fuel with respect to the number of grid elements are depicted in Figure 5. Investigations are carried out with an injection pressure of 135 MPa, and a back pressure of 5 MPa. Figure 5 shows that the mass flow rate of the liquid fuel reaches a constant value when the mesh size is 3 μm (115,558 elements), so this mesh size is used to solve the internal flow of the nozzle.

In all of the simulations, the needle is considered stationary. This is a suitable assumption since the needle is completely open more than 90% of the injection time [35]. The flow inside the nozzle is assumed to be transient and incompressible. The total injection time is 0.7 ms, and the time step is varied from 1e-8 s in initial steps to 1e-7 s in final steps. In this study, a standard European diesel fuel is used and its properties are presented in Table 1.

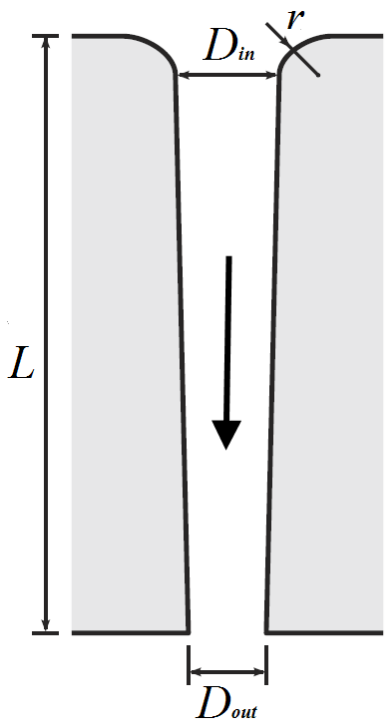

Fig4. Geometrical parameters of the orifice.

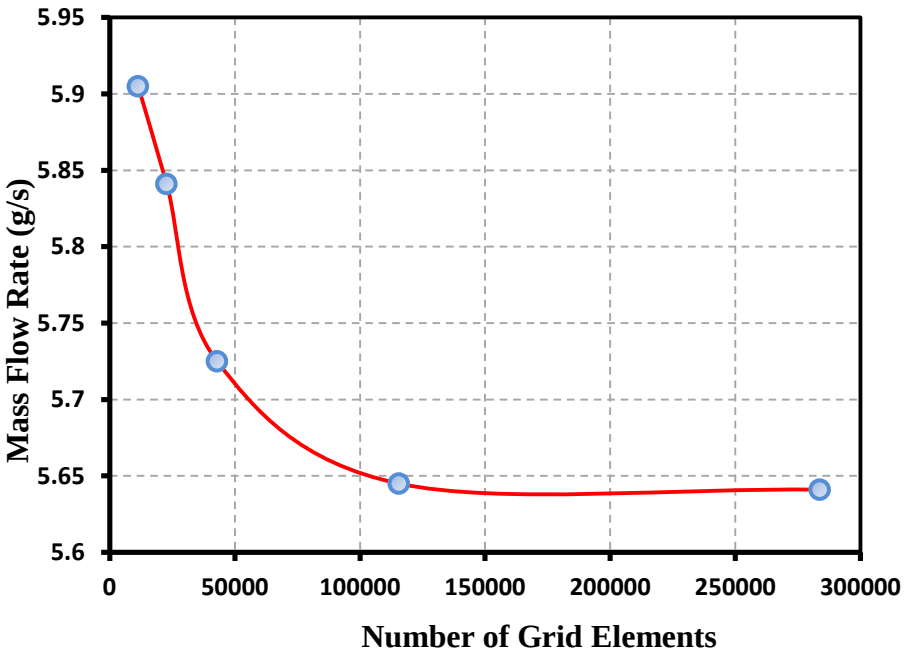

Fig5. Variation of the mass flow rate of the liquid fuel with respect to the number of grid elements

6. Results and discussion

In this section, simulation results related to the internal flow of the single-hole nozzle are presented, and the effects of dynamic and geometrical parameters on the internal nozzle flow and the cavitation phenomenon are discussed. In order to present the results, the discharge coefficient and vapor volume fraction contour are used. The discharge coefficient is used to characterize the internal flow of the nozzle, and the vapor volume fraction contour is used to express the amount and distribution of cavitation in the nozzle.

6.1 Effect of the injection pressure

Investigating the characteristics of the internal nozzle flow in different injection pressures is of great importance. In this study, the injection pressure is increased from 10 MPa to 250 MPa while the back pressure is fixed at 5 MPa. To investigate the effect of the injection pressure, the variation of the discharge coefficient with respect to the cavitation number is depicted in Figure 6. For high values of K (higher than 1.50), the discharge coefficient is almost constant, and the nozzle flow is non-cavitating; the Reynolds number is higher than 12,000 and the flow is turbulent. By increasing the injection pressure, bubbles appear in the inlet edge. For cavitation numbers between 1.15-1.50, the fluid flow, after detaching from wall, reattaches to wall because there is not enough pressure gradient. In this region, because cavitation does not develop to the nozzle outlet, the outlet area does not change, and the discharge coefficient remains constant. As the cavitation number decreases, the vapor phase reaches the outlet of the nozzle and decreases the outlet area, resulting in the decrease of the discharge coefficient. This region of the flow is called supercavitation.

The vapor volume fraction contours of the specified points on Figure 6 related to different injection pressures are depicted in Figure 7. At the injection pressure of 10 MPa, there is no cavitation in the nozzle. Approaching to the injection pressure of 15 MPa, bubbles appear in the inlet edge of the orifice. At the injection pressure of 20 MPa, cavitation is developing toward the outlet of the nozzle. At the injection pressure of 40 MPa, cavitation has developed to the outlet of the nozzle. By increasing the injection pressure, the amount of the vapor phase increases at the outlet, and the discharge coefficient decreases.

6.2 Effect of the back pressure

Another effective dynamic parameter on the internal flow of the nozzle is back pressure. In this study, the back pressure is varied from 0.5 MPa to 9 MPa. The effect of back pressure is investigated at two different injection pressures, 35 MPa and 135 MPa. In this section, in addition to discharge coefficient, mass flow rate of the liquid fuel is used to present the results. Variations of the discharge coefficient and the mass flow rate of the fuel with cavitation number (K) are plotted in Figure 8 for two different injection pressures. Values of the back pressure are specified on the figure. Trend of variations of the discharge coefficient and the mass flow rate is different in Figure 8(a) and (b). For the injection pressure of 35 MPa, as the cavitation number decreases (the back pressure decreases), the mass flow rate increases while the discharge coefficient remains constant since cavitation has not started yet. As the back pressure decreases more, diagram reaches a point, corresponding to p_{back} = 3 MPa, where the mass flow is constant. At this point, as the vapor reaches the orifice outlet, the choked flow phenomenon occurs, and the downstream does not affect the upstream. In this situation, although the pressure difference increases, the mass flow rate remains constant while the discharge coefficient decreases. For the injection pressure of 135 MPa, the mass flow rate is constant for all values of the back pressure since the injection pressure is high, and the flow is choked for all of the back pressures.

Volume fraction contours of the vapor phase are depicted in Figure 9 for different back pressures. Figure 9(a) shows that how at the injection pressure of 35 MPa bubbles form in the orifice, and the flow is choked when the back pressure decreases from 9 MPa to 3 MPa. On the other hand, at the injection pressure of 135 MPa, for all values of the back pressure, the flow is choked (see Figure 9(b)).

In the following, the effects of geometrical parameters on the internal nozzle flow are studied. Geometrical parameters include inlet curvature radius of the orifice, orifice conicity, and its length which are shown in Figure 4.

6.3Effect of the orifice inlet curvature radius

The inlet curvature radius of the orifice is usually represented by r/D_{in}. The effect of the inlet curvature radius of the orifice is studied when the above mentioned ratio is varied from 0 to 0.3. To increase r/D_{in}, only the inlet curvature radius is increased while other geometrical parameters are kept constant.

The injection pressure is 135 MPa , and the back pressure is 5 MPa . Variation of the discharge coefficient with respect to r/D_{in} is shown in Figure 10. As can be seen, increasing the inlet curvature radius of the orifice results in increasing the discharge coefficient. The increase in the discharge coefficient is because of the decrease in pressure drop. When the inlet curvature radius increases, resistance to flow decreases, and less pressure drop is occurred at this point; as a result, cavitation decreases, and the effective area increases, resulting in increasing the discharge coefficient. Volume fraction contours of the vapor phase are depicted in Figure 11 for five different curvature radii. For the nozzle with a sharp inlet edge, cavitation develops to the outlet. As the inlet curvature radius increases, the cavitation gradually decreases. For r/D_{in} = 0.3, vapor almost disappears.

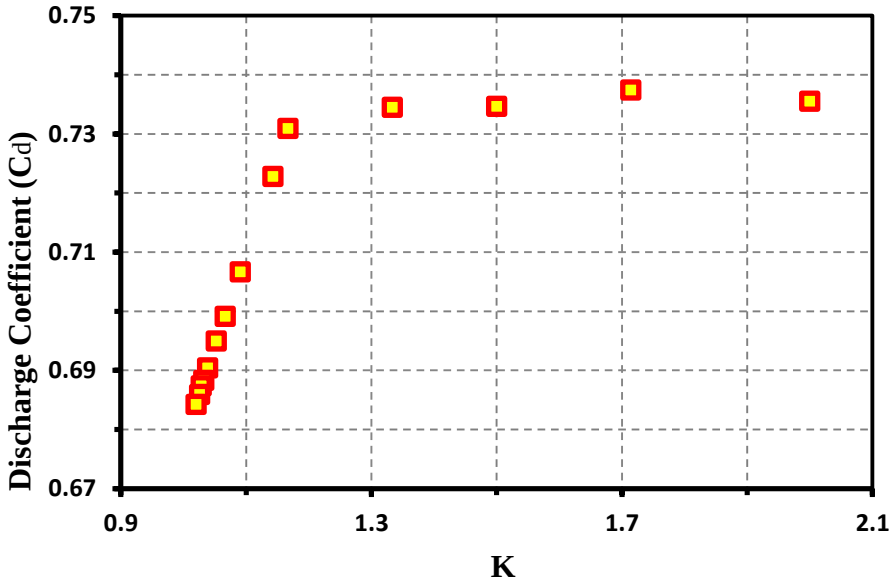

Fig6. Diagram of the discharge coefficient with respect to the cavitation number.

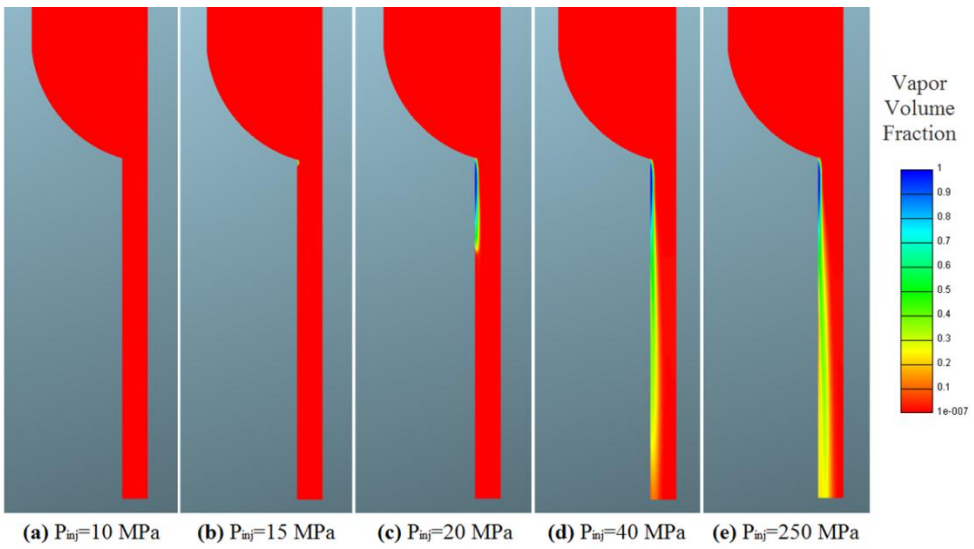

Fig7. Contours of vapor volume fraction for different injection pressures.

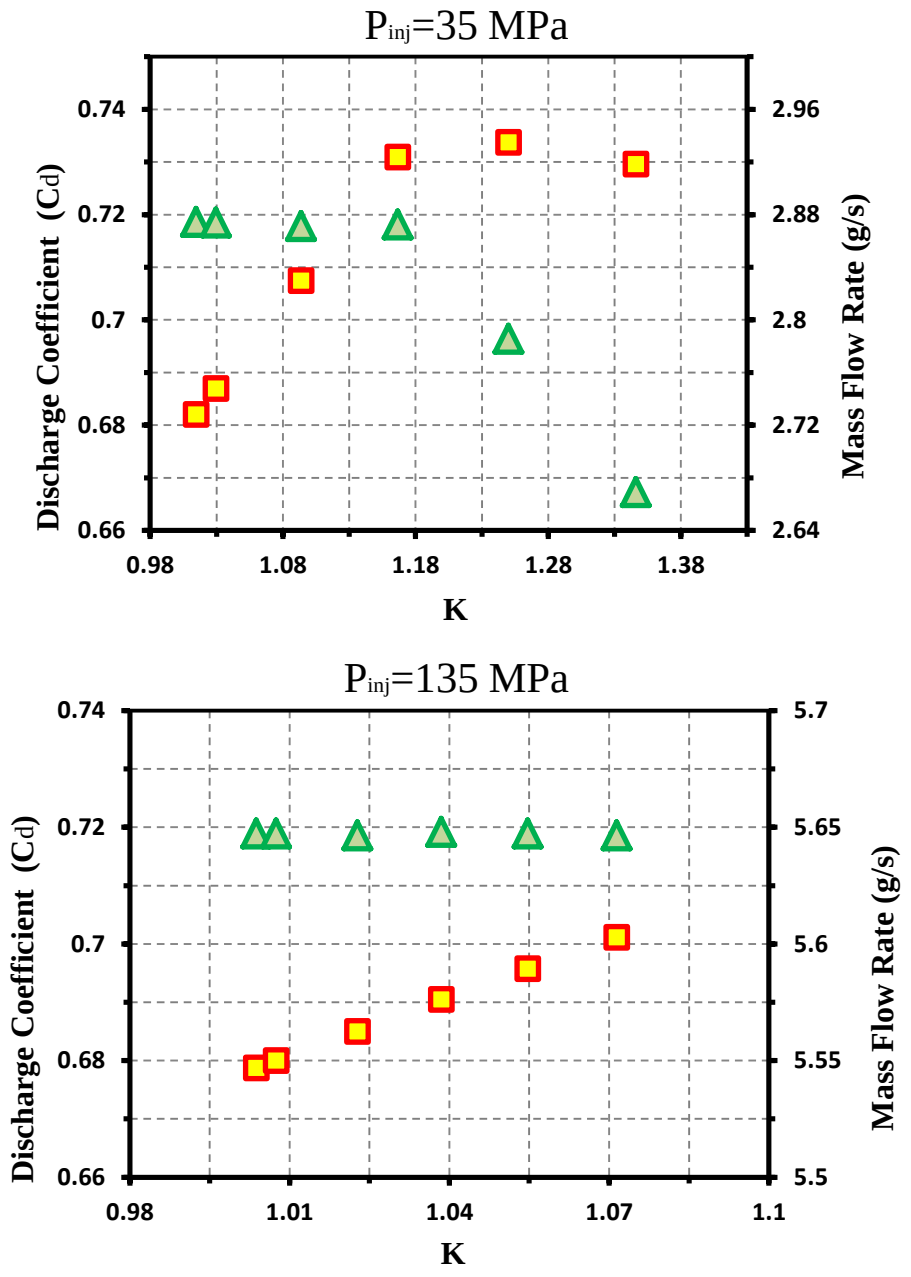

Fig8..Diagram of the discharge coefficient and mass flow rate with respect to the cavitation number. (a), p_{inj} = 35 MPa (b), p_{inj} = 135 MPa.

6.4 Effect of the orifice iconicity

Orifice conicity is defined using the $k-factor$ parameter as follows:

$$k-factor=\frac{D_{in}-D_{out}}{10\ (\mu m)} \qquad (12)$$

Where, D_{in} and D_{out} are in microns. In this article, the effect of orifice conicity is investigated with a $k-factor$ of -3, 0 and 3. In order to vary the $k-factor$, the outlet diameter of the orifice is considered to be constant while the inlet diameter is changed. For example, for an orifice with $k-factor$ = 3, the inlet diameter is 180 µm. Other geometrical parameters are the same as the base nozzle. Investigations are carried out with an injection pressure of 135 MPa, and a back pressure of 5 MPa. Volume fraction contours of the vapor phase for three

orifices with different conicity are presented in Figure 12. The convergent orifice cavitates less compared to the cylindrical orifice, and there is only a little vapor at its inlet edge. However, in the divergent orifice, cavitation intensity is higher than that of the cylindrical one, and the vapor occupies almost all the outlet area. This is due to the fact that the convergent nozzle increases flow uniformity, which causes flow disturbances to decrease and lowers the cavitation intensity. Figure 13 shows the dependence of the discharge coefficient on the orifice iconicity.

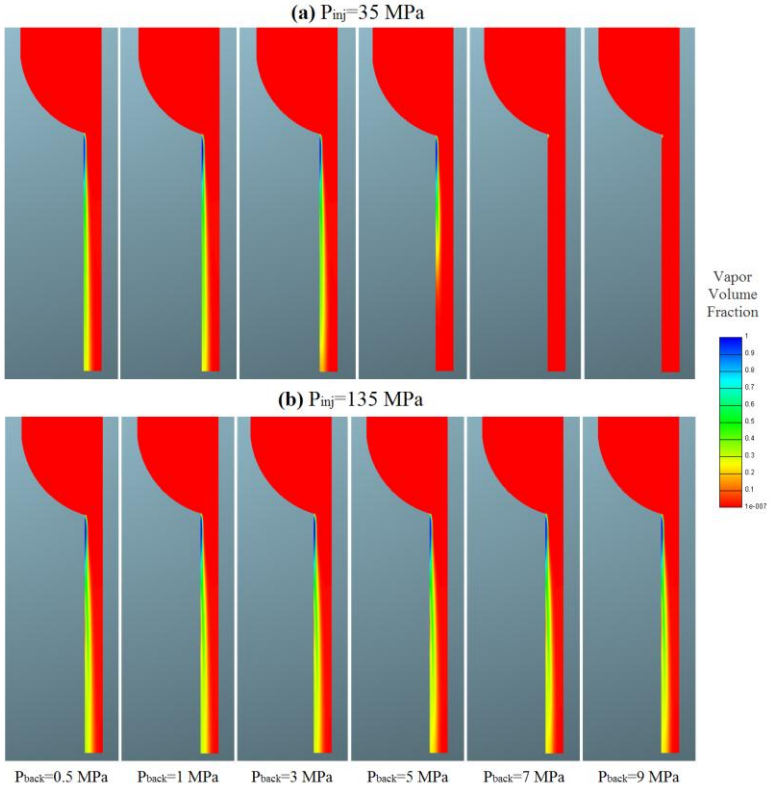

Fig9. Contours of vapor volume fraction for different back pressures. (a), p_{inj} = 35 MPa (b), p_{inj} = 135 MPa.

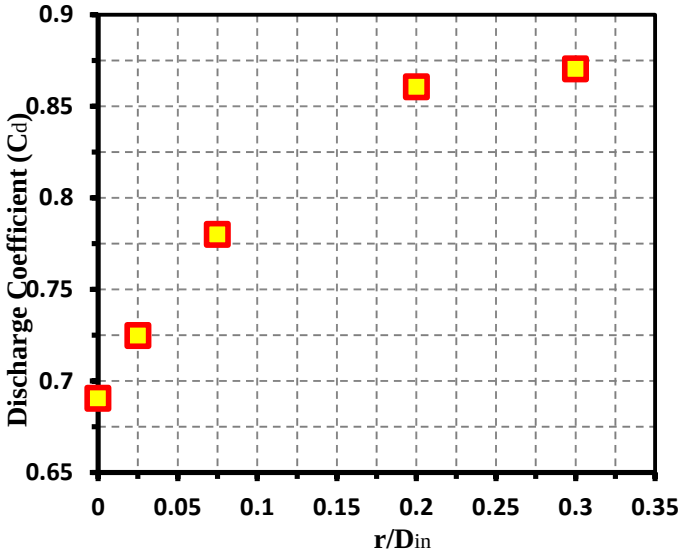

Fig10. Diagram of the discharge coefficient with respect to r/D_{in}.

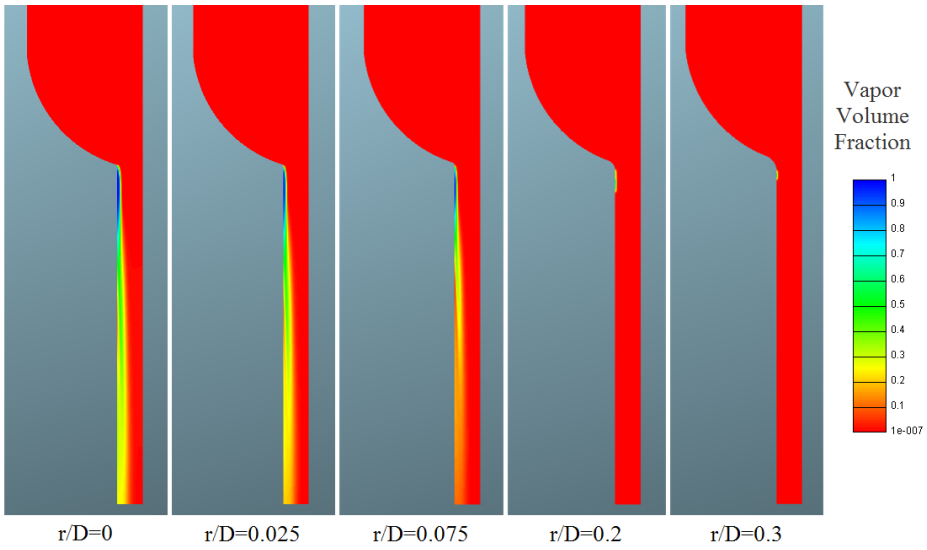

Fig11. Contours of vapor volume fraction for differentr/D_{in}

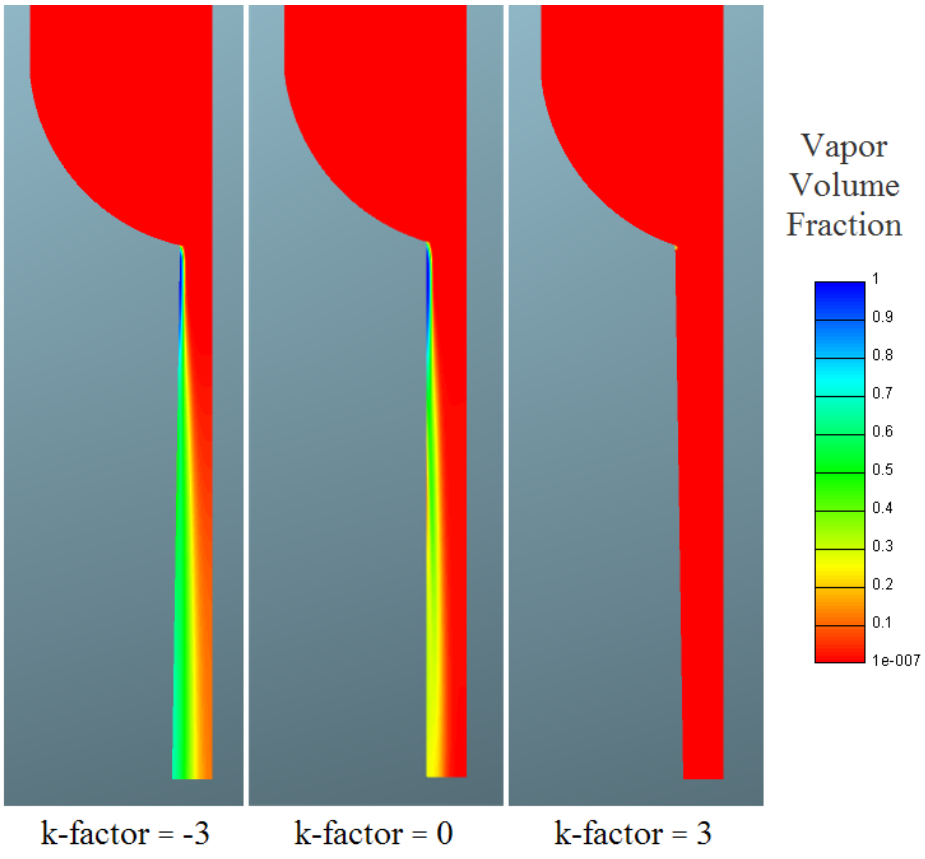

Fig12. Contours of vapor volume fraction for different $k-factor$.

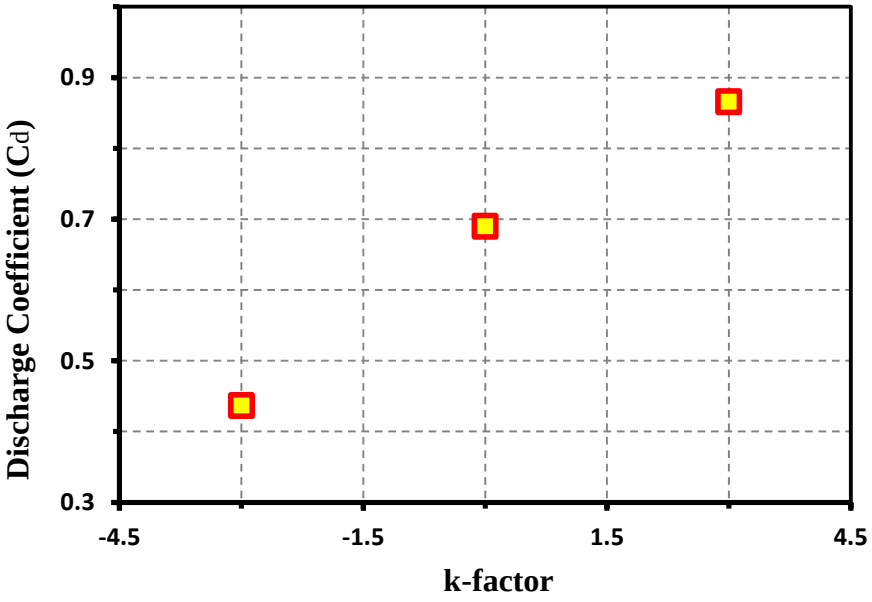

Fig13. Diagram of the discharge coefficient with respect to $k-factor$.

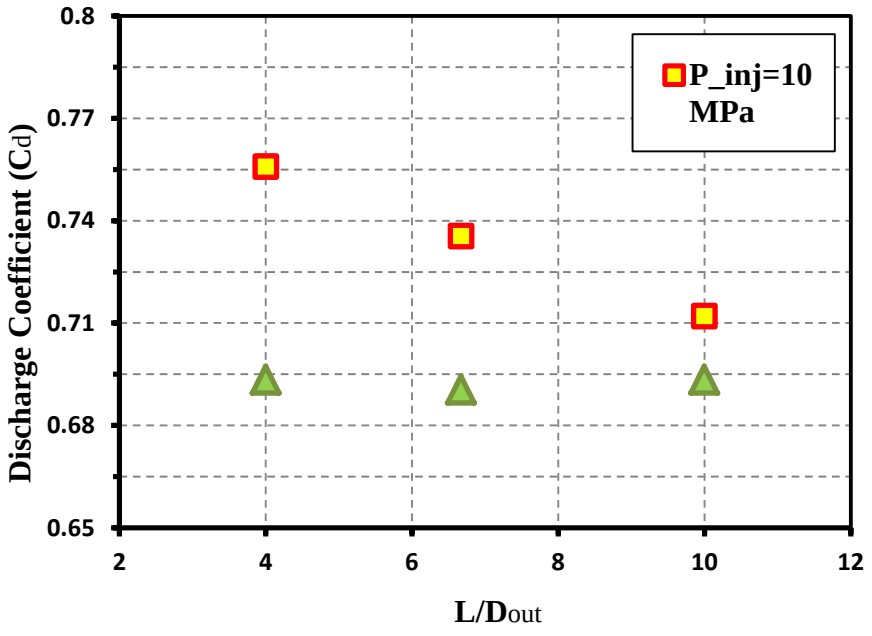

Fig14. Diagram of the discharge coefficient with respect to L/D_{out}.

6.5.Effect of the orifice length

The length of the orifice is usually represented by L/D_{out}. In order to study the effect of the orifice length, L/D_{out} is varied from four to 10. L/D_{out} is increased by increasing the length while other geometrical parameters are as same as the base nozzle. Investigations are carried out with two different injection pressures of 10 MPa and 135 MPa, and a back pressure of 5 MPa. Variations of the

discharge coefficient with L/D_{out} are shown in Figure 14 for both of the injection pressures. At the pressure of 135 MPa, increasing the length does not have a considerable effect on the discharge coefficient, and the discharge coefficient remains almost constant. At the pressure of 10 MPa , increasing length results in a noticeable decrease in the discharge coefficient. This is because of the type of the flow inside the orifice. Volume fraction contours of the vapor phase are depicted in Figure 15. At the pressure of 10 MPa, the flow is non-cavitating, so the liquid fuel is in contact with the orifice wall (see Figure 15(a)). In this situation, longer orifice will have more friction losses, leading to lower discharge coefficient. At the pressure of 135 MPa , supercavitation happens in the orifice, and the vapor develops to the outlet of the orifice (Figure 15(b)). In this situation, because the flow detaches from the wall, there is no contact between the liquid fuel and the solid wall, and increasing the length has no impact on friction losses. At the pressure of 135 MPa, flow structure is the same for all nozzles, and all of them experience supercavitation, so there is no qualitative difference between various nozzles. The most important difference is the amount of the vapor at the outlet; in a way that, the amount of vapor at the outlet for longer orifices is less than that of the shorter ones. At the pressure of 10 MPa, the flow is non-cavitating for all nozzles.

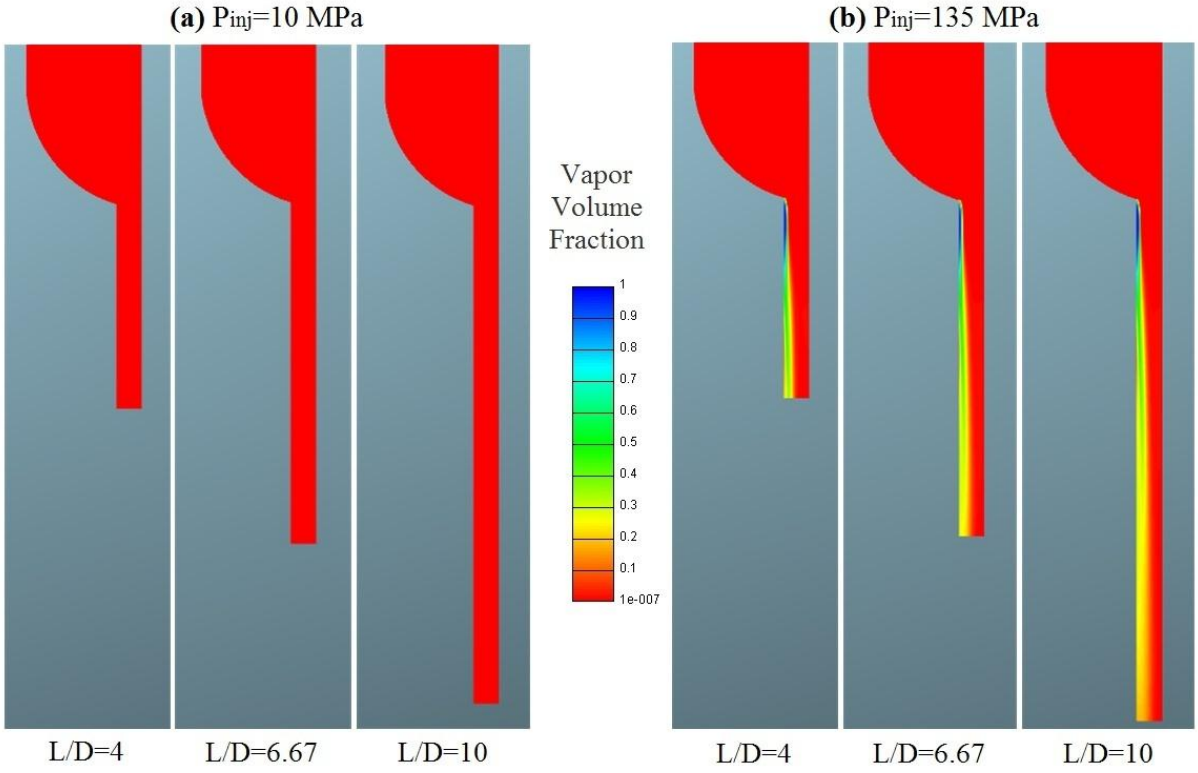

Fig15. Contours of vapor volume fraction for different L/D_{out}. (a), p_{inj} = 10 MPa (b), p_{inj} = 135 MPa.

2. 7.Conclusions

In the present work, the cavitation phenomenon in an injector nozzle is simulated using the Eulerian-Eulerian two-fluid method. The effects of dynamic and geometrical parameters on the cavitational flow of the nozzle are investigated. Based on the results, the following conclusions are redrawn:

1. As the injection pressure increases and the cavitation develops, the amount of the vapor phase at the outlet of the nozzle increases which results in the decrease in the discharge coefficient. Moreover, the flow regime inside the nozzle changes by increasing the injection pressure. The flow regime at lower pressures is noncavitational, and then, it is cavitation

inception. At higher pressures, the flow regime changes to developing cavitation and then to supercavitation.

2. The effect of the back pressure on the nozzle flow depends on the difference between the inlet and the outlet pressures. At lower levels of pressure difference where the flow is in noncavitational or cavitation inception condition, lowering the back pressure increases the mass flow rate. In this situation, since the cavitation does not develop to the outlet of the nozzle, the discharge coefficient remains constant. At high enough levels of pressure difference, because of the occurrence of the choked flow phenomenon, the back pressure does not affect the characteristics of the internal nozzle flow like mass flow rate, and cavitation quality. In this situation, since the cavitation develops to the outlet of the nozzle, the discharge coefficient decreases as the back pressure is lowered.

3. As the inlet curvature radius of the orifice increases, resistance to flow decreases and less pressure drop occurs at this point. As the pressure drop decreases, the cavitation intensity decreases, and as a result, the effective area increases which leads to increasing the discharge coefficient. Conicity of the orifice has a similar effect as the inlet curvature radius of the orifice. Increasing the conicity of the orifice increases the uniformity of the flow. Increasing the uniformity of the flow decreases the disturbances of the flow; it, also, decreases the cavitation intensity, and consequently, increases the discharge coefficient. The effect of the orifice length on the internal nozzle flow depends on the flow regime. If the orifice is in a noncavitational condition, friction losses increase as the length of the orifice increases, and the discharge coefficient decreases. Nevertheless, if the nozzle is in supercavitational condition, because of the flow detachment, there is no contact between the liquid fuel and the solid surface. So, increasing the length of the orifice does not have any considerable effects on either the friction losses or the discharge coefficient.

References

[1]. Tullis, J.P. (1989) Hydraulics of Pipelines: Pumps, Valves, Cavitation, Transients; New York: John Wiley & Sons.

[2]. Som, S., Aggarwal, S.K., El-Hannouny, E.M., and Longman, D.E. (2010) Engineering for Gas Turbines and Power, 132: 1-12.

[3]. Mulemane, A., Subramaniyam, S., Lu, P., Han, J. et al. (2004) SAE Technical Paper, No. 2004-01-0027.

[4]. Chaves, H., Knapp, M., Kubitzek, A., Obermeier, F. et al. (1995) SAE Technical Paper, No. 950290.

[5]. Schmidt, D.P. and Corradini, M.L. (1997) Atomization and Sprays, 7(6):603-616.

[6]. Osman, A. (2006) Engineering Failure Analysis, 13:1126-1133.

[7]. Yan, C.L. and Aggarwal, S.K. (2006) Engineering for Gas Turbines and Power, 128(3):482-492.

[8]. Faeth, G.M., Hsiang, L.P., and Wu, P.K. (1995) International Journal of Multiphase Flow, 21:99-127.

[9]. Tonini, S., Gavaises, M., Theodorakakos, A., and Cossali, G.E. (2010) Proceedings of IMechE Part D: Journal of Automobile Engineering, 224(1):125–141.

[10]. Arcoumanis, C., Gavaises, M., and French, B. (1997) SAE Technical Paper, No. 970799.

[11]. You, Y., Powell, C.F., Poola, R., Wang, J., and Schaller, J.K. (2001) Atomization and Sprays, 11:471-490.

[12]. Salvador, F.J., Hoyas, S., Novella, R., and Martínez-LÓpez, J. (2011) Proceedings of IMechE Part D: Journal of Automobile Engineering, 225(4):545-563.

[13]. He, Z., Bai, J., Wang, Q., Mu, Q., and Huang, Y. (2010) ASME 3rd Joint US-European Fluids Engineering Summer Meeting, Montreal, August 1–5.

[14]. Bergwerk, W. (1959) Proceeding of the Institution of Mechanical Engineers, 173(25):655-660.

[15]. Nurick, E.H. (1976) Fluids Engineering, 98:681-687.

[16]. Soteriou, C., Smith, M., and Andrews, R. (1995) SAE Technical Paper, No. 950080.

[17]. He, L. and Ruiz, F. (1995) Atomization and Sprays, 5:569-584.

[18]. Badock, C., Wirth, R., Fath, A., and Leipertz, A.M. (1999) International Journal of Heat and Fluid Flow, 20:538-544.

[19]. Arcoumanis, C., Flora, H., Gavaises, M., and Badami, M. (2000) SAE Technical Paper, No. 2000-01-1249.

[20]. Winklhofer, E., Kull, E., Kelz, E., and Morozov, (2001) Proceedings of the ILASS-Europe Conference, Zurich, September 2-6.

[21]. Benajes, J., Pastor, J.V., Payri, R., and Plazas, A.H. (2004) Fluids Engineering, 126:63-71.

[22]. Payri, F., Bermudez, V., Payri, R., and Salvador, F.J. (2004) Fuel, 83:419-431.

[23]. Roth, H., Giannadakis, E., Gavaises, M., Arcoumanis, C., Omae, K., Sakata, I.,

Nakamura, M., and Yanagihara, H. (2005) SAE Technical Paper, No. 2005-01-1237.
[24]. Powell, C.F., Kastengren, A.L., Liu, Z., and Fezzaa, K. (2011) Engineering for Gas Turbines and Power, 133(1):521-529.
[25]. Payri, F., Payri, R., Salvador, F.J., and Martínez-López, J. (2012) Computers & Fluids, 58:88-101.
[26]. Lockett, R.D., Liverani, L., Thaker, D., Jeshani, M., and Tait, N.P. (2013) Fuel, 106:605-616.
[27]. Giannadakis, E. (2005) Modeling of Cavitation in Automotive Fuel Injector Nozzles, PhD Thesis, Imperial College, London, UK.
[28]. Avl List GmbH. (2008) AVL Fire V. 2008: CFD Solver, Eulerian Multiphase.
[29]. Alajbegovic, A., Grogger, H.A., and Philipp, H. (1999) Proceedings of the 12th Annual Conference on Liquid Atomization and Spray Systems, Indianapolis, May 16-19.
[30]. Alajbegovic, A., Meister, G., Greif, D., and Basara, B. (2002) Experimental Thermal and Fluid Science, 26:677-681.
[31]. Sato, Y. and Sekoguchi, K. (1975) International Journal of Multiphase Flow, 2:79-95.
[32]. Brennen, C.E. (2005) Fundamentals of Multiphase Flows; Cambridge: Cambridge University Press.
[33]. Franklin, R.E. and McMillan, J. (1984) Fluids Engineering, 106(3):336-341.
[34]. Ishii, M. (1975) Thermo Fluid Dynamic Theory of Two-Phase Flow; Paris: Eyrolles.
[35]. Som, S. (2009) Development and Validation of Spray Models for Investigating Diesel Engine Combustion and Emissions, PhD Thesis, University of Illinois at Chicago, USA.
[36]. Perry, R.H. and Green, D.W. (1997) Perry's Chemical Engineers' Handbook; New York: McGraw-Hill.
[37]. Battistoni, M. and Grimaldi, C.N. (2010) SAE International Journal of Fuels and Lubricants, 3(2):879-900.